Available online at www.sciencedirect.com

ScienceDirect

Physics Procedia 69 (2015) 404 – 412

Physics Procedia

10th World Conference on Neutron Radiography 5-10 October 2014

Three-Dimensional Imaging of Magnetic Domains with Neutron Grating Interferometry

I. Manke[a,*], N. Kardjilov[a], R. Schäfer[b], A. Hilger[a], R. Grothausmann[a,c], M. Strobl[a,d], M. Dawson[a,e], Ch. Grünzweig[f], Ch. Tötzke[a,i], Ch. David[f], A. Kupsch[g], A. Lange[g], M. P. Hentschel[g], J. Banhart[a,h]

[a]*Helmholtz Centre Berlin for Materials and Energy (HZB), 14109 Berlin, Germany*
[b]*Leibniz Institute for Solid State and Materials Research (IFW) Dresden, 01069 Dresden, Germany*
[c]*Hannover Medical School (MHH), 30625 Hannover, Germany*
[d]*European Spallation Source (ESS), SE-221 00 Lund, Sweden*
[e]*University of Salford, Salford, M5 4WT, UK*
[f]*Paul Scherrer Institut, 5232 Villigen-PSI, Switzerland*
[g]*Federal Institute for Materials Research and Testing (BAM), 12200 Berlin, Germany*
[h]*Technische Universität Berlin, 10623 Berlin, Germany*
[i]*University of Potsdam, 14476 Potsdam-Golm, Germany*

Abstract

This paper gives a brief overview on 3D imaging of magnetic domains with shearing grating neutron tomography. We investigated the three-dimensional distribution of magnetic domain walls in the bulk of a wedge-shaped FeSi single crystal. The width of the magnetic domains was analyzed at different locations within the crystal. Magnetic domains close to the tip of the wedge are much smaller than in the bulk. Furthermore, the three-dimensional shape of individual domains was investigated. We discuss prospects and limitations of the applied measurement technique.

Selection and peer-review under responsibility of Paul Scherrer Institut

Keywords: neutron imaging; tomography; magnetic domains; grating interferometry; darkfield imaging; shearing gratings; Talbot-Lau; three-dimensional data quantification; tomographic reconstruction

* Corresponding author. Tel.: +49-30-8062-42682; fax: +49-30-8062-42098.
E-mail address: manke@helmholtz-berlin.de

Selection and peer-review under responsibility of Paul Scherrer Institut
doi:10.1016/j.phpro.2015.07.057

1. Introduction

Neutron imaging has become an extensively used measurement technique on various fields [1-9]. It plays an important role in the investigation of engineering materials and components, e.g. in fuel cell research where it has already become a well-established method [10-18]. The sensitivity of polarized neutrons to magnetic fields allows for two- and three-dimensional imaging of magnetic fields [19-25]. However, visualization of magnetic bulk domains with such a polarized neutron imaging setup is difficult because of the high strength of magnetic fields within magnetic domains of most materials [26-28]. Some years ago grating interferometric imaging with X-rays and neutrons was introduced by Pfeiffer et al [29, 30]. Grating interferometric imaging is an arising measurement technique providing access to structural information of samples that is hardly accessible by other methods. In combination with neutrons it is possible to visualize magnetic domain walls within the bulk of a material [31-34]. Neutrons are scattered by magnetic domain walls contributing to the so-called "darkfield" signal. Strobl et al. have shown that the neutron darkfield signal can be exploited for reconstructing three-dimensional (tomographic) data sets [35-38]. Two years later Manke et al. presented a modified measurement mode that allows for the reconstruction of three-dimensional images revealing the distribution of magnetic domains within a bulk material [39].

The aim of this paper is to give a brief overview on neutron darkfield imaging of magnetic bulk domains [39].

2. Experimental setup

2.1. Neutron Imaging Instrument

The measurements were performed at the CONRAD/V7 instrument at the BER II research reactor (Helmholtz Centre Berlin for Materials and Energy, HZB)[40]. The research reactor BER II is a light water reactor with about 10 MW thermal power. Close to the reactor a cold neutron beam source operating at about 25 K is installed. The tomography instrument CONRAD/V7 is located at the end of a curved neutron guide that is attached to the cold neutron source. The main advantage of the curved guide is the elimination of most of the high energy neutrons, i.e. thermal and epithermal neutrons, and of gamma radiation.

An adaptable detector setup was used for the presented measurements and the spatial resolution adjusted to about 35 µm [41]. However, it should be noted that the resolution strongly depends on the geometry of the installed grating setup being the main limiting factor.

2.2. Grating Set-Up

A shearing-grating setup was installed in front of the detector of the CONRAD/V7 instrument as shown in figure 1 [39]. Such a grating setup consists of at least three different gratings: A source grating G0, a phase grating G1 and an absorption grating G2 [30, 42]. A schematic drawing of such a setup is shown in figure 2. The sample can be located at different positions. For the tomographic measurement it was placed between G1 and G2 [39]. The details about phase grating interferometric imaging are described e.g. by Pfeiffer et al. [29, 30, 42]. The gratings were manufactured by Ch. Grünzweig and Ch. David at Paul Scherrer Institute (Villigen, Switzerland). The manufacturing process is described by Grünzweig et al. [43].

2.3. Tomographic measurement

The exposure time for each radiographic projection (2048x2048 pixels) was 100 s (90 s in the case of the FeSi steel sheet). During each scan 14 images (16 images in case of the FeSi steel sheet) were taken (over 1 period) [39]. The overall measurement time for a single G_2 scan was about 30 min. All datasets were corrected by background and flat field images. For evaluation of the neutron dark-field images a sinusoidal fitting routine was applied. The tomographic reconstruction included 100 of such image sets recorded in equidistant angular steps over a range of 360°.

Fig. 1. Shearing-grating setup at CONRAD instrument. The round-shaped phase grating can be seen in the center.

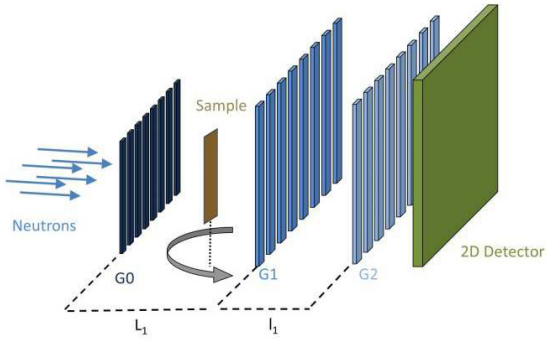

Fig. 2. Schematic drawing of a typical shearing-grating setup for interferometric imaging.

2.4. Samples

For detailed description of the FeSi steel investigated in radiographic mode we refer to Grünzweig et al.[32]. Subject of the tomographic investigation was a FeSi single crystal (Fe 12.8-at%Si) with a cylindrical wedge shape. The diameter was about 7 mm and the length about 15 mm. It was grown by zone melting and later cut to a wedge-shaped sample by an electro-erosive saw [39]. Starting from the tip, the width of the wedge increases from 0 mm to 7 mm over a distance of about 14 mm.

2.5. Tomographic data reconstruction and visualization

We applied an iterative reconstruction algorithm (DIRECTT), which is especially suited for so-called “incomplete” data sets [44-48]. Three-dimensional visualization and rendering was completed using commercial software (AVIZO and VGStudioMax).

3. Results

3.1. Radiography

Fig. 3 shows the attenuation contrast and the darkfield contrast image of a FeSi steel sheet. Since the steel sheet has a constant thickness no features can be seen in the attenuation contrast image (Fig. 3 (a)). Even the spherical shape of sample is only slightly visibly. However, neutrons scattered at domain walls are revealed by the darkfield

signal (Fig 3 (b)). The dark vertical stripes can be assigned to individual magnetic domain walls. Close to the center of the sample the domain width is decreasing in accordance with the findings of Grünzweig et al. [32].

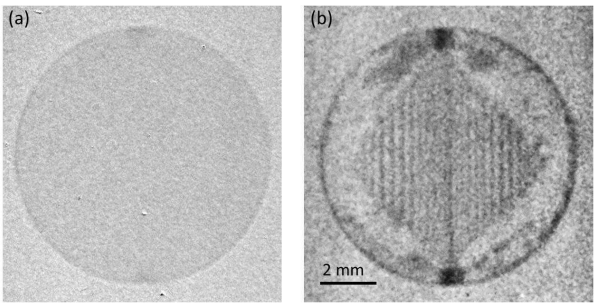

Fig. 3. Absorption contrast image (a) and darkfield image (b) of a FeSi sheet.

3.2. Tomography

Using the example of a wedge-shaped FeSi single crystal it is illustrated how the radiographic measurement technique can be extended to three dimensional (tomographic) imaging of magnetic domains. The fundamental challenge of this approach is that the domain walls are only visible if they are aligned almost parallel to the incident neutron beam. Therefore, in a single radiographic projection image only a small amount of the domain walls is revealed. During tomographic data acquisition, the sample is stepwise rotated. At each angle position different domains become visible. After a full rotation of 360° all domain walls became visible at least two times (Note: in the case of a 180° tomography only once). The angle dependent visibility of domain walls is a very challenging problem for conventional tomographic reconstruction algorithms, i.e. the filtered back-projection algorithm (FBP). Although FBP gives still acceptable results, we decided to use a more sophisticated although time consuming procedure that is called DIRECTT and that provides some advantages over FBP.

A horizontal slice through the reconstructed tomogram of the FeSi wedge is shown in Fig. 4. The white lines are assigned to magnetic domain walls. The walls are not arbitrarily orientated but prefer certain directions mainly the main axes of the crystal, i.e. (100), (010) and (001) (see Hubert & Schäfer and Schäfer et al. for further details)[26, 28]. This image also reveals that the width values of the different magnetic domains (at least of the larger ones) are very close to each other, i.e. some values can be found more frequently than others.

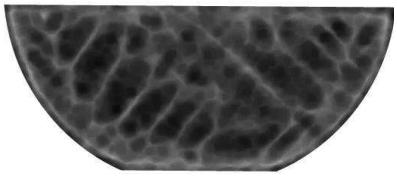

Fig. 4. Cross section through the shearing grating neutron tomogram of a FeSi single crystal [39].

This finding was analyzed in more detail in Figure 5 (a), where slices through the tomogram were taken at different positions of the tapered section of the FeSi crystal. It can be seen that the domain widths are correlated to the crystal width, i.e. magnetic domain widths are increasing with increasing crystal width. Just for illustration two additional cross sections through the tomogram along two different arbitrarily chosen planes are given in figure 5 (b).

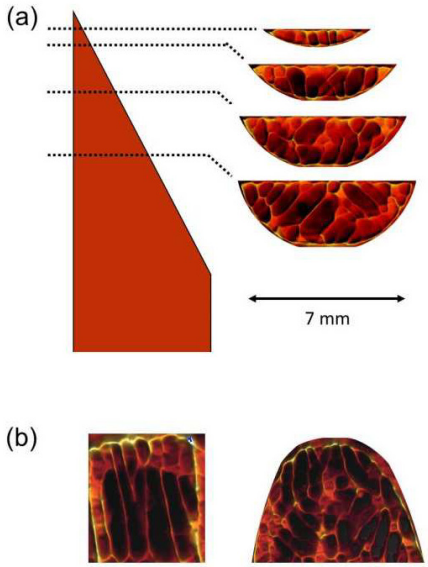

Fig. 5. (a) Horizontal tomographic cross sections at different locations within the wedge-shaped FeSi single crystal. (b) Two additional cross sections at arbitrary angles through the wedge [39].

3.3. Data quantification

Aim of the presented tomographic investigation was the verification of a theory on the correlation between magnetic domain widths and crystal size as described in Hubert & Schäfer [26, 39]. For a quantitative analysis of the magnetic domains the data set was binarized applying a certain grey value threshold. This allows for the separation of individual magnetic domains as shown in figure 6.

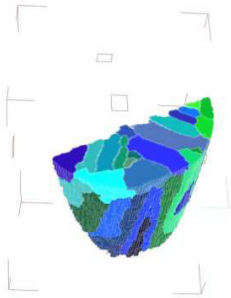

Fig. 6. 3D view on the segmented magnetic domains within the FeSi wedge (Note: The colors are only used for visual separation of the magnetic domains.).

Individual magnetic domains could be extracted from the data set and analyzed individually. One of the magnetic domains extracted at a certain location (marked in figure 7 (a)) is shown in Fig. 7 (b) from three different viewing angles. Although the geometric shape of a magnetic domain seems to be very complicated, it is still possible to define a domain width for a certain location within the magnetic domain.

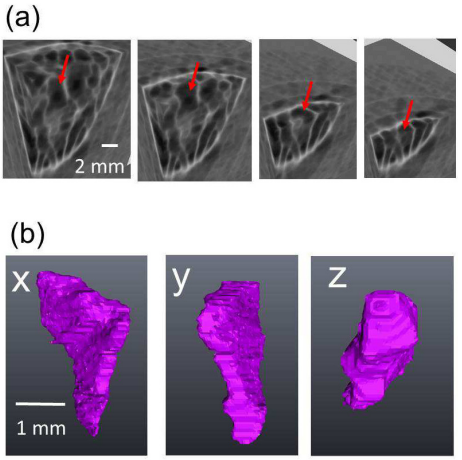

Fig. 7. (a) 3D view into the tip of the wedge revealing the magnetic domain shapes. (b) Single magnetic domain extracted from the tomogram at the location marked by red arrows in (a) [39].

The domain size analysis revealed that the domain width W is increasing with the crystal thickness D as follows [39]:

$$W \sim \sqrt{D} \tag{1}$$

However, this equation is only valid for domain sizes above ~ 100 µm. In fact the correlation is more complex. The general correlation of bulk domain width W_b and crystal width D can be described by the following equation:

$$D = 2W_b^2\left(\frac{C_p}{\gamma_w} + \frac{2C_s}{G_m C_s W_b + \gamma_w}\right) \tag{2}$$

where γ_w is the specific wall energy, C_p is the "quasi-closure" coefficient, C_s a geometry-dependent factor and G_m describes the maximum rate (speed) of the domain width that is rising from its surface width W_s to its bulk value W_b. A detailed explanation of this result and of the correlation between domain width and crystal thickness are given by Hubert & Schäfer [26, 39].

4. Discussion

Neutron darkfield imaging with shearing gratings (or grating interferometry) can be used to visualize the magnetic domain walls in the bulk of a FeSi single crystal three-dimensionally. The quality of the 3D data is sufficient for detailed analysis of the magnetic domain shapes and structures. However, also some of the drawbacks of the measurement technique should be mentioned. Measurement times are comparably long. It takes several days for a full tomography with acceptable signal-to-noise ratio. Typical spatial resolutions are between 70-150 µm. This is still not sufficient, because the domain shapes are blurred by the limited resolution and data quantification becomes very difficult. Owing to fundamental properties of the darkfield signal the projection data set is not suited for conventional tomographic reconstruction algorithms, although reconstruction results with FBP are still acceptable.

5. Summary/Outlook

We demonstrated the possibilities of neutron darkfield tomography to analyze magnetic domains in 3D. The quantitative investigation of the magnetic domains in a FeSi single crystal revealed a correlation between crystal width and domain widths as predicted by Hubert & Schäfer [26]. The major drawbacks of the technique are the comparably long measurement times of several days and the still limited spatial resolution of about 70-150 µm.

In future, optimized grating setups may drastically reduce the required measurement times, e.g. by higher visibility values. The introduction of novel high resolution imaging detection setups with high light through-put will further improve the quality of data sets [49, 50]. Furthermore, the installation of new imaging stations, e.g. at the European Spallation Source in Sweden [51], could provide much higher neutron fluxes, that may reduce measurement times to a few hours in future.

Acknowledgements

The authors would like to thank G. Behr for the preparation of the FeSi single crystal.

References

[1] N. Kardjilov, I. Manke, A. Hilger, M. Strobl, Banhart J. Neutron imaging in materials science. Materials Today 2011;14:248.
[2] Strobl M, Manke I, Kardjilov N, Hilger A, Dawson M, Banhart J. Advances in neutron radiography and tomography. Journal of Physics D-Applied Physics 2009;42:243001.
[3] Banhart J, editor Advanced Tomographic Methods in Materials Research and Engineering. Oxford, UK: Oxford University Press, 2008.
[4] Schillinger B, Lehmann E, Vontobel P. 3D neutron computed tomography: requirements and applications. Physica B: Condensed Matter 2000;276-278:59.
[5] Schillinger B, Bücherl T. ZfP-Zeitung. ZfP-Zeitung pp , 2004;89:34.
[6] Lehmann E. Recent improvements in the methodology of neutron imaging. Pramana Journal of Physics 2008;71:653.
[7] Lehmann EH, Josic L, Frei G. Material Research with Neutron Imaging Methods at SINQ. Neutron News 2009;20:20.
[8] Vontobel P, Lehmann EH, Hassanein R, Frei G. Neutron tomography: Method and applications. Physica B: Condensed Matter 2006;385-386:475.
[9] Kaestner AP, Hartmann S, Kuhne G, Frei G, Grunzweig C, Josic L, Schmid F, Lehmann EH. The ICON beamline - A facility for cold neutron imaging at SINQ. Nucl Instrum Meth A 2011;659:387.
[10] Lehmann EH, Boillat P, Scherrer G, Frei G. Fuel cell studies with neutrons at the PSI's neutron imaging facilities. Nuclear Instruments and Methods in Physics Research Section A: Accelerators, Spectrometers, Detectors and Associated Equipment 2009;605:123.
[11] Bellows RJ, Lin MY, Arif M, Thompson AK, Jacobson D. Neutron Imaging Technique for In Situ Measurement of Water Transport Gradients within Nafion in Polymer Electrolyte Fuel Cells. Journal of The Electrochemical Society 1999;146:1099
[12] Arif M, Jacobson DL, Hussey DS. Neutron Imaging Study of the Water Transport in Operating Fuel Cells. FY 2006 Annual Progress Report. 2006. p.875.
[13] Hussey DS, Jacobson DL, Arif M, Coakley KJ, Vecchia DF. In Situ Fuel Cell Water Metrology at the NIST Neutron Imaging Facility. Journal of Fuel Cell Science and Technology 2010;7:021024.
[14] Hickner MA, Siegel NP, Chen KS, Hussey DS, Jacobson DL, Arif M. In Situ High-Resolution Neutron Radiography of Cross-Sectional Liquid Water Profiles in Proton Exchange Membrane Fuel Cells. Journal of The Electrochemical Society 2008;155:B427.
[15] Hickner MA, Siegel NP, Chen KS, McBrayer DN, Hussey DS, Jacobson DL, Arif M. Real-Time Imaging of Liquid Water in an Operating Proton Exchange Membrane Fuel Cell. Journal of The Electrochemical Society 2006;153:A902.
[16] Ch. Tötzke, Manke I, Arlt T, Markötter H, Kardjilov N, Hilger A, Krüger P, Hartnig C, Scholta J, Banhart J. High resolution large area neutron imaging detector for fuel cell research. Journal of Power Sources 2011;196:4631.
[17] Klages M, Enz S, Markotter H, Manke I, Kardjilov N, Scholta J. Investigations on dynamic water transport characteristics in flow field channels using neutron imaging techniques. Journal of Power Sources 2013;239:596.
[18] Markotter H, Manke I, Kuhn R, Arlt T, Kardjilov N, Hentschel MP, Kupsch A, Lange A, Hartnig C, Scholta J, Banhart J. Neutron tomographic investigations of water distributions in polymer electrolyte membrane fuel cell stacks. Journal of Power Sources 2012;219:120.
[19] Kardjilov N, Manke I, Strobl M, Hilger A, Treimer W, Meissner M, Krist T, Banhart J. Three-dimensional imaging of magnetic fields with polarized neutrons. Nature Physics 2008;4:399.
[20] Dawson M, Manke I, Kardjilov N, Hilger A, Strobl M, Banhart J. Imaging with polarized neutrons. New Journal of Physics 2009;11:043013.
[21] Manke I, Kardjilov N, Strobl M, Hilger A, Banhart J. Investigation of the skin effect in the bulk of electrical conductors with spin-polarized neutron radiography. Journal of Applied Physics 2008;104:076109.

[22] Strobl M, Treimer W, Walter P, Keil S, Manke I. Magnetic field induced differential neutron phase contrast imaging. Applied Physics Letters 2007;91:254104.
[23] Strobl M, Pappas C, Hilger A, Wellert S, Kardjilov N, Seidel SO, Manke I. Polarized neutron imaging: A spin-echo approach. Physica B: Condensed Matter 2011;406:2415.
[24] Schulz M, Neubauer A, Muhlbauer M, Calzada E, Schillinger B, Pfleiderer C, Boni P. Polarized Neutron Radiography with a Periscope. In: Goll G, Lohneysen HV, Loidl A, Pruschke T, Richter M, Schultz L, Surgers C, Wosnitza J, editors. International Conference on Magnetism, vol. 200. 2010.
[25] Schulz M, Schmakat P, Franz C, Neubauer A, Calzada E, Schillinger B, Böni P, Pfleiderer C. Neutron depolarisation imaging: Stress measurements by magnetostriction effects in Ni foils. Physica B: Condensed Matter 2010;doi:10.1016/j.physb.2010.10.079.
[26] Hubert A, Schäfer R, editors. Magnetic Domains: Springer, 1998.
[27] Libovick.S. SPATIAL REPLICA OF FERROMAGNETIC DOMAINS IN IRON-SILICON ALLOYS. Phys Status Solidi A 1972;12:539.
[28] Schafer R, Schinnerling S. Bulk domain analysis in FeSi-crystals. Journal of Magnetism and Magnetic Materials 2000;215:140.
[29] Pfeiffer F, Weitkamp T, Bunk O, David C. Phase retrieval and differential phase-contrast imaging with low-brilliance x-ray sources. Nature Physics 2006;2:258.
[30] Pfeiffer F, Grunzweig C, Bunk O, Frei G, Lehmann E, David C. Neutron phase imaging and tomography. Physical Review Letters 2006;96.
[31] Grunzweig C, David C, Bunk O, Dierolf M, Frei G, Kuhne G, Kohlbrecher J, Schafer R, Lejcek P, Ronnow HMR, Pfeiffer F. Neutron decoherence imaging for visualizing bulk magnetic domain structures. Physical Review Letters 2008;101.
[32] Grunzweig C, David C, Bunk O, Dierolf M, Frei G, Kuhne G, Schafer R, Pofahl S, Ronnow HMR, Pfeiffer F. Bulk magnetic domain structures visualized by neutron dark-field imaging. Applied Physics Letters 2008;93:112504.
[33] Grunzweig C, David C, Bunk O, Kohlbrecher J, Lehmann E, Lai YW, Schafer R, Roth S, Lejcek P, Kopecek J, Pfeiffer F. Visualizing the propagation of volume magnetization in bulk ferromagnetic materials by neutron grating interferometry (invited). Journal of Applied Physics 2010;107.
[34] Lee SW, Kim KY, Kwon OY, Kardjlov N, Dawson M, Hilger A, Manke I. Observation of Magnetic Domains in Insulation-Coated Electrical Steels by Neutron Dark-Field Imaging. Applied Physics Express 2010;3:106602.
[35] Strobl M, Grünzweig C, Hilger A, Manke I, Kardjilov N, David C, Pfeiffer F. Neutron Dark-Field Tomography. Physical Review Letters 2008;101:123902.
[36] Hilger A, Kardjilov N, Kandemir T, Manke I, Banhart J, Penumadu D, Manescu A, Strobl M. Revealing microstructural inhomogeneities with dark-field neutron imaging. Journal of Applied Physics 2010;107:036101.
[37] Strobl M. General solution for quantitative dark-field contrast imaging with grating interferometers. Sci. Rep. 2014;4.
[38] Strobl M, Hilger A, Kardjilov N, Ebrahimi O, Keil S, Manke I. Differential phase contrast and dark field neutron imaging. Nuclear Instruments and Methods in Physics Research Section A: Accelerators, Spectrometers, Detectors and Associated Equipment 2009;605:9.
[39] Manke I, Kardjilov N, Schäfer R, Hilger A, Strobl M, Dawson M, Grünzweig C, Behr G, Hentschel M, David C, Kupsch A, Lange A, Banhart J. Three-dimensional imaging of magnetic domains. Nature Communications 2010;1:125.
[40] Kardjilov N, Hilger A, Manke I, Strobl M, Dawson M, Williams S, Banhart J. Neutron tomography instrument CONRAD at HZB. Nuclear Instruments and Methods in Physics Research Section A: Accelerators, Spectrometers, Detectors and Associated Equipment 2011;651:47.
[41] Kardjilov N, Dawson M, Hilger A, Manke I, Strobl M, Penumadu D, Kim KH, Garcia-Moreno F, Banhart J. A highly adaptive detector system for high resolution neutron imaging. Nuclear Instruments and Methods in Physics Research Section A: Accelerators, Spectrometers, Detectors and Associated Equipment 2011;651:95.
[42] Pfeiffer F, Bech M, Bunk O, Kraft P, Eikenberry EF, Bronnimann C, Grunzweig C, David C. Hard-X-ray dark-field imaging using a grating interferometer. Nature Materials 2008;7:134.
[43] Grunzweig C, Pfeiffer F, Bunk O, Donath T, Kuhne G, Frei G, Dierolf M, David C. Design, fabrication, and characterization of diffraction gratings for neutron phase contrast imaging. Review of Scientific Instruments 2008;79.
[44] Lange A, Kupsch A, Hentschel MP, Manke I, Kardjilov N, Arlt T, Grothausmann R. Reconstruction of limited CT data of fuel cell components using DIRECTT. Journal of Power Sources 2010;196:5293.
[45] Kupsch A, Lange A, Hentschel MP, Manke I, Kardjilov N, Arlt T, Grothausmann R. Reconstruction of limited CT data sets of fuel cells with Directt. Materials Testing 2010;52:676.
[46] Lange A, Hentschel MP, Kupsch A, Hilger A, Manke I, Luck S, Schmidt V, Grothausmann R. Reduction of Missing Wedge Artifacts in Computerised Tomography by DIRECTT. Materials Testing 2014;56:716.
[47] Grothausmann R, Zehl G, Manke I, Fiechter S, Bogdanoff P, Dorbandt I, Kupsch A, Lange A, Hentschel MP, Schumacher G, Banhart J. Quantitative Structural Assessment of Heterogeneous Catalysts by Electron Tomography. J. Am. Chem. Soc. 2011;133:18161.
[48] Lange A, Hentschel MP, Kupsch A. Computed tomography reconstructions by DIRECTT-2D model calculations compared to filtered backprojection. Materials Testing-Materials and Components Technology and Application 2008;50:272.
[49] Williams SH, Hilger A, Kardjilov N, Manke I, Strobl M, Douissard PA, Martin T, Riesemeier H, Banhart J. Detection system for microimaging with neutrons. Journal of Instrumentation 2012;7:P02014.
[50] Lehmann EH, Frei G, Kuhne G, Boillat P. The micro-setup for neutron imaging: A major step forward to improve the spatial resolution. Nucl Instrum Meth A 2007;576:389.

[51] A. Hilger, Kardjilov N, Manke I, Zendler C, Lieutenant K, Habicht K, Banhart J, Strobl M. Neutron guide optimisation for a time-of-flight neutron imaging instrument at the European Spallation Source. Optics Express 2015;to be published.